

Direct numerical simulation of turbulent flows in a wall-normal rotating channel

NAN-SHENG LIU and XI-YUN LU*

Department of Modern Mechanics, University of Science and Technology of China, Hefei,
Anhui 230026, People's Republic of China

Direct numerical simulation (DNS) is carried out to study turbulence characteristics in a wall-normal rotating channel with the rotation number N_r from 0 to 0.12 and the Reynolds number 194 based on the friction velocity of the non-rotating case and the half-height of the channel. Based on the present calculated results, two typical rotation regimes are identified. When in weak rotation regime with $0 < N_r < 0.05$, turbulence statistics correlated with the spanwise velocity fluctuation are enhanced since the shear rate of the spanwise mean flow induced by the Coriolis force increases, but other statistics are suppressed. When in strong rotation regime with $N_r > 0.05$, all the turbulence statistics decrease as the effect of the Coriolis force plays a dominant role. The budgets of transport equations for the Reynolds stresses are calculated to reveal the effect of the Coriolis force on the dynamic process of turbulent kinetic energy production, dissipation and redistribution. With the increase of N_r in weak rotation regime, the main mechanism for the generation of the streamwise turbulent energy is gradually altered from the shear production effect related to the streamwise mean flow to the energy redistribution due to the pressure strain correlation. Correspondingly, the generation of the spanwise turbulent energy also changes from the energy redistribution effect to the shear production of the spanwise mean flow. In strong rotation regime, the mean flow shear rate is found to be a key factor to the turbulence production and dissipation. The redistribution between the streamwise and spanwise components of turbulent kinetic energy due to the effect of the Coriolis force becomes weak. A remarkable change of the direction of the near-wall vortical structures, nearly in alignment with the absolute mean flow direction, is observed. An attempt to evaluate the mean spacing between the streaky structures and the angle between the wall structures and streamwise direction has been examined based on the two-point correlations of the velocity fluctuations to reveal the change of the near-wall structures.

1. Introduction

Rotating turbulent flow widely exists in various industrial, geophysical and astrophysical applications. In these flows, the rotation induces additional body forces, i.e. centrifugal and Coriolis forces, acting on the turbulent flow, so that the momentum mechanism becomes more complicated. Understanding the mechanism of turbulent flow in a rotating system is of great importance in applications and fundamentals.

Turbulent channel flow subjected to the wall-normal rotation is a typical problem. Such a flow is quite different from that in a widely studied spanwise rotating channel, which is characterized by the augmentation and damping of turbulence in the pressure and suction sides, respectively, and the identification of large-scale rotation-induced roll cells due to Taylor–Görtler instability [1–5]. Since the mean vorticity component perpendicular to the rotating

*Corresponding author. E-mail: xlu@ustc.edu.cn

axis appears in the wall-normal rotating channel flow, turbulence is found to be more sensitive to the wall-normal rotation, even though weak system rotation can induce a significant spanwise mean velocity [6]. As a result, the absolute mean flow deviates from the initial streamwise direction, which makes all the six components of the Reynolds stress tensor nonzero and redirects the mean flow and the turbulence structures. According to the findings [7], the interaction between the vorticity of coherent structures and the background vorticity due to the imposed wall-normal rotation can significantly change the near-wall turbulence behaviour. Recently, Wu and Kasagi [8] studied numerically the effect of the wall-normal rotation, combined with the streamwise or spanwise rotation, on turbulence characteristics at low rotation number. Our recent work also provided insight into the rotation effect on some salient features of swirling and rotational flows [9, 10].

This problem is similar to the prototype of the atmospheric planetary boundary layer, which depends on the Reynolds number based on the geostrophic wind speed aloft and the Ekman layer e-folding depth and the rotation number based on the normal component of the Earth's angular velocity [11, 12]. According to the Taylor–Proudman theorem, turbulent flow subjected to a strong rotation will undergo a transition towards two-dimensional turbulence and eventually towards a re-laminarized flow, which was verified experimentally. In this situation, the turbulence dissipation rate becomes very weak and contributes little to the budget of turbulent kinetic energy [13]. The coherent structures are verified to be more sensitive to the Coriolis force effect induced by the wall-normal rotation [7].

Here, direct numerical simulation (DNS) is employed to investigate the rotation effect on the wall-normal rotating turbulent channel flows for the rotation number ranging from low to high value, especially on the dynamic process of turbulent kinetic energy and the near-wall coherent structures. Our goal in this study is to examine the turbulence statistics, budgets of turbulent kinetic energy and flow structures.

This paper is organized as follows. The mathematical formulation is described in section 2. The numerical method and its validation are briefly given in section 3. In section 4, some typical results including the turbulence statistics and structures are discussed. The budgets of the Reynolds stress tensor are analysed to reveal the wall-normal rotation effect on the dynamic processes of turbulent kinetic energy. Finally, concluding remarks are summarized in section 5.

2. Mathematical formulation

2.1 Governing equations

The governing equations for the turbulent flow through a wall-normal rotating channel are the incompressible Navier–Stokes equations. To normalize the equations, the friction velocity u_τ of the non-rotating channel flow is used as the velocity scale, and the half-height of the channel h as the length scale. Then the non-dimensional equations are given as

$$\frac{\partial u_i}{\partial x_i} = 0 \quad (1)$$

$$\frac{\partial u_i}{\partial t} + \frac{\partial u_i u_j}{\partial x_j} = -\frac{\partial p}{\partial x_i} + \delta_{1i} + \frac{1}{Re_\tau} \frac{\partial^2 u_i}{\partial x_j \partial x_j} - N_\tau \varepsilon_{ijk} \frac{\Omega_j}{\Omega} u_k \quad (2)$$

where p represents the effective pressure combined with the centrifugal force. The non-dimensional parameters in this problem are the rotation number and the Reynolds number,

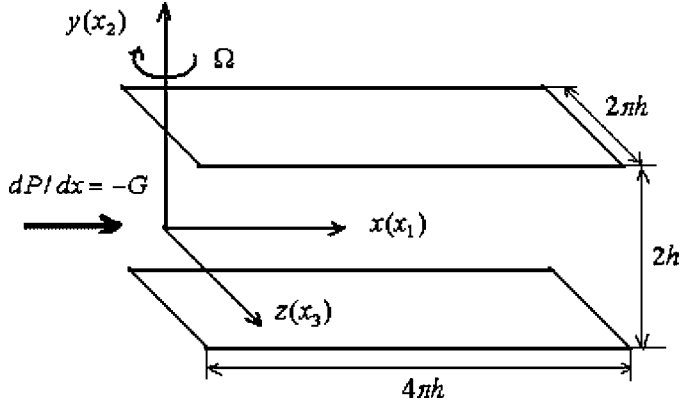


Figure 1. Configuration of the wall-normal rotating channel flow.

which are defined as $N_\tau = 2\Omega h/u_\tau$ and $Re_\tau = u_\tau h/\nu$, respectively, with Ω being the angular velocity of a rotating frame and ν the kinematic viscosity.

As shown in figure 1 for the sketch of the wall-normal rotating channel, the turbulent flow between two parallel infinite walls is driven by a constant streamwise pressure gradient equal to that of the non-rotating case. The no-slip boundary condition is set on the walls and periodic boundary conditions are employed in the streamwise and spanwise directions.

2.2 Solutions of wall-normal rotating laminar channel flow

In the laminar flow through a wall-normal rotating channel, the streamwise and spanwise velocity components, i.e. U and W , satisfy the equations deduced by Ekman [14] for wind-driven laminar flow above a horizontal plane subjected to the Earth's rotation, which can be rewritten as

$$N_\tau U = \frac{1}{Re_\tau} \frac{d^2 W}{dy^2} \quad (3)$$

$$-N_\tau W = 1 + \frac{1}{Re_\tau} \frac{d^2 U}{dy^2}. \quad (4)$$

Once the no-slip condition is employed to the walls, the solution for equations (3) and (4) can be obtained as

$$U(y) = -\frac{\text{sh}[k'(y+1)] \sin[k'(y-1)] + \text{sh}[k'(y-1)] \sin[k'(y+1)]}{N_\tau (\text{ch}2k' + \cos 2k')} \quad (5)$$

$$W(y) = \frac{\text{ch}[k'(y+1)] \cos[k'(y-1)] + \text{ch}[k'(y-1)] \cos[k'(y+1)]}{N_\tau (\text{ch}2k' + \cos 2k')} - \frac{1}{N_\tau} \quad (6)$$

where $k' = \sqrt{Re_\tau N_\tau / 2}$. Equations (5) and (6) indicate that both U and W vanish as the rotation number approaches to infinity. It means that the fluid in the channel rotates like a rigid body in this limit case. When the wall-normal rotation is weak, the streamwise velocity U is positive over the channel, while it also changes its sign in the core region of the channel at certain rotation number. The spanwise velocity W is always negative.

Figures 2(a) and (b) show the distributions of the streamwise and spanwise velocities evaluated by use of (5) and (6) for the rotation number from 0 to 0.2 and the Reynolds number $Re_\tau = 194$. It is observed that U is reduced significantly as the rotation number increases and

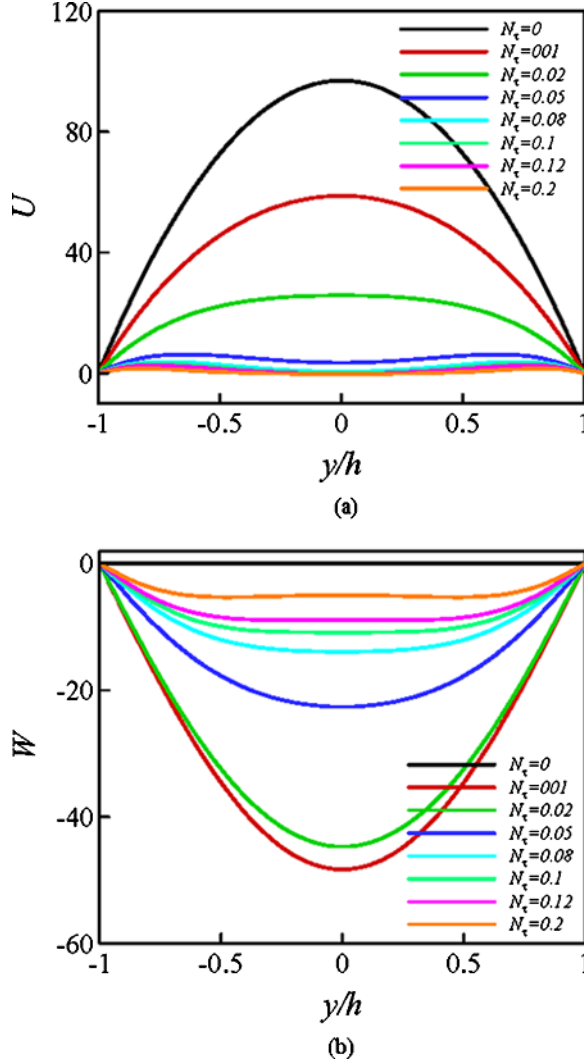


Figure 2. Profiles of the velocity for the laminar flow through the wall-normal rotating channel: (a) streamwise; (b) spanwise component.

even becomes a small negative value in the core region of the channel subjected to a strong rotation (e.g. $N_\tau = 0.12$, and 0.2). However, the Coriolis force enhances the spanwise velocity W in the weak rotation case (e.g. $N_\tau = 0.01$) and suppresses it remarkably at higher rotation number. According to these features, the rotation number is chosen as from 0.01 to 0.12 in this study to examine the effect of the Coriolis force on the turbulent flows.

3. Numerical method

To solve the incompressible Navier–Stokes equations (1) and (2), a fractional-step method developed by Orlandi [15] is used. Spatial derivatives are discretized by a second-order central difference. Time advancement is carried out by the semi-implicit scheme using the Crank–Nicholson scheme for the viscous terms and the three-stage Runge–Kutta scheme for the convective terms. The discretized formulation was described in detail by Orlandi [15]. This

method simplifies the boundary condition of the non-solenoidal velocity field, while remains the feature of the algorithm developed by Kim and Moin [16] and Rain and Moin [17], and has the additional advantage that the minimum amount of computer run-time memory is realized.

In the present study, the Reynolds number Re_τ is chosen as 194, which is the same as that used by Kristoffersen and Andersson [4] in their DNS of the spanwise rotating channel flow. The mesh number is $193 \times 161 \times 129$ with the corresponding computational domain $4\pi h \times 2h \times 2\pi h$ in the streamwise, wall-normal and spanwise directions, respectively. According to Kim *et al.* [18], this grid system is enough to resolve all essential scales of the low-Reynolds-number turbulence and contains the largest scale structures in the channel. A stretching transformation is employed to obtain fine grid resolution in the wall regions. The grid point next to the wall is located at $y^+ = 0.3$ approximately, while the largest spacing is about $\Delta y^+ = 4.5$ in the centre of the channel, where y^+ is defined as $y^+ = (1 - |y/h|)Re_\tau$. Uniform grids are employed in the streamwise and spanwise directions with the grid spacing $\Delta x^+ = 12.6$ and $\Delta z^+ = 9.5$, respectively. To exhibit the computational domain size being large enough in the wall-normal rotating turbulent channel flow, typical profiles of two-point correlations of the velocity fluctuations at $y^+ = 5.4$ are shown in figures 3(a)–(f). It is seen that these correlations approach negligibly small values, indicating that the computational domain used is large enough.

It is worthwhile to mention that the performance and reliability of the numerical method used here have been verified extensively based on the DNS of rotating and non-rotating turbulent pipe flows [19, 20]. It was ensured that the second- and higher-order turbulence statistics compared well with available DNS results calculated by the spectral methods and experimental data. Extensive studies have confirmed that the numerical approach with the second-order accuracy schemes succeeded in predicting turbulence characteristics. Meanwhile, the relevant code and method used have been verified in our previous work [21–24]. Thus, it is confirmed that the numerical approach used here is reliable to predict turbulence characteristics in a wall-normal rotating channel.

4. Results and discussion

4.1 Mean velocity

The profiles of the mean velocity in the streamwise and spanwise directions are shown in figures 4(a) and (b), where y_d denotes the distance from the wall, i.e. $y_d = 1 - |y|/h$, and the bracket $\langle \rangle$ represents the average in time and in the horizontal plane. Figure 4 exhibits the redirecting of the mean flow in the wall-normal rotating channel. As the rotation is imposed, the streamwise mean velocity $\langle u \rangle$ decreases monotonically with the increase of N_τ , indicating the reduction of the wall shear rate related to the streamwise mean flow. The behaviour of the streamwise mean velocity varying with N_τ is consistent with that predicted analytically in figure 2(a), but the negative value of $\langle u \rangle$ disappears in the core region of the channel at high rotation number, e.g. $N_\tau = 0.12$, as predicted in the laminar flow case. As shown in figure 4(b), the spanwise mean velocity $\langle w \rangle$ increases when N_τ varies from 0 to 0.08; however, when N_τ increases further, e.g. $N_\tau = 0.1$ and 0.12, the spanwise mean flow is suppressed obviously. The behaviour of $\langle u \rangle$ and $\langle w \rangle$ varying with N_τ can be explained by the fact that the Coriolis force, induced by the wall-normal rotation, is balanced not only by the viscous shear stress of the mean flow but also by the Reynolds stress related to the velocity fluctuations in the rotating turbulent channel flow. Differently, in the laminar flow case, it is only balanced by the mean flow shear stress. Note that, as shown in figure 4(b), the wall shear rate of the spanwise mean

flow at $N_\tau = 0.05$ is somewhat larger than those for other cases, which is responsible for the feature of turbulence statistics correlated with the spanwise velocity fluctuation and will be discussed in the following.

The absolute mean flow direction is shown in figure 4(c), where the angle θ_f is defined as $\theta_f = \tan^{-1}(|\langle w \rangle / \langle u \rangle|)$, i.e. the angle of the absolute mean flow with respect to the streamwise direction. The angle increases when the rotation rate increases. The absolute mean flow deviates from the streamwise direction with the acute angle θ_f about 62° in the wall region and more than 75° in the core region of the channel at $N_\tau = 0.12$. It is noticed that the absolute mean flow at $N_\tau = 0.05$ is tilting to the spanwise direction with an angle $\theta_f \approx 45^\circ$ in the core region.

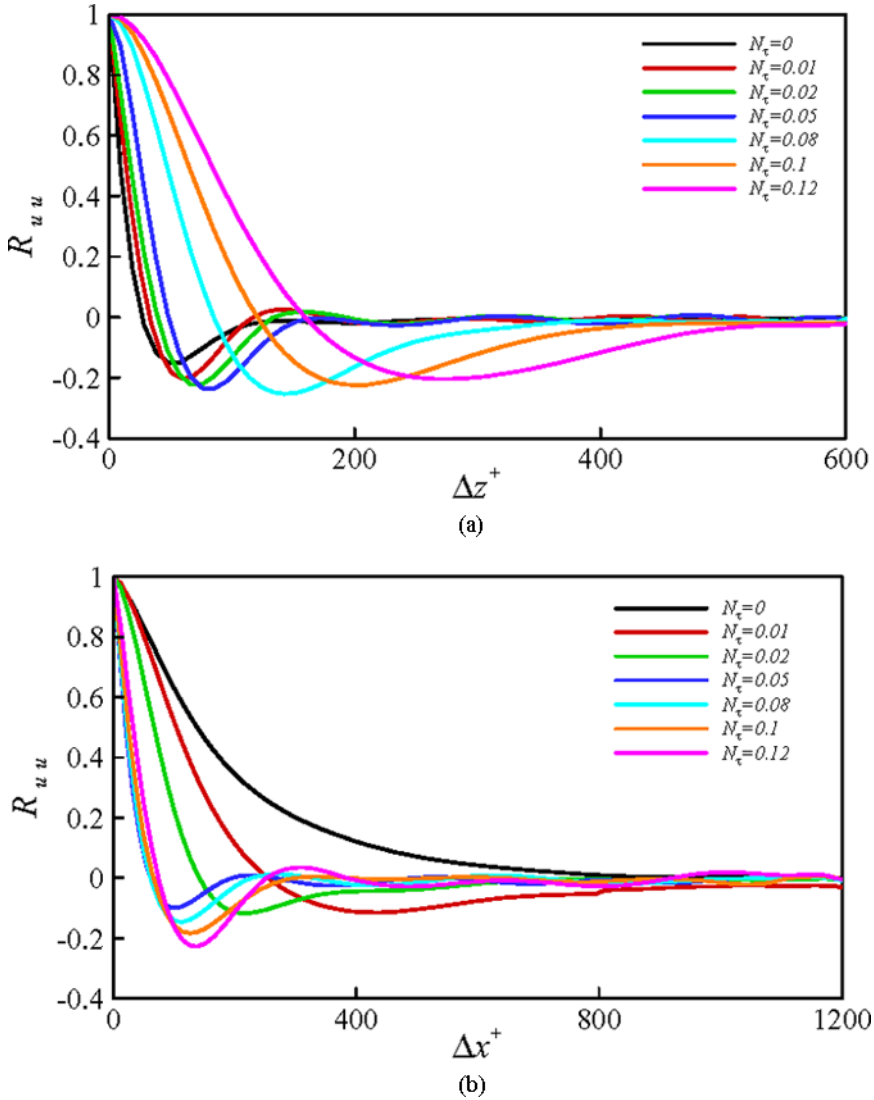


Figure 3. Two-point correlations along the homogeneous directions at $y^+ = 5.4$: (a) R_{11} along the spanwise direction (or spanwise); (b) R_{11} , streamwise; (c) R_{22} , spanwise; (d) R_{22} , streamwise; (e) R_{33} , spanwise; (f) R_{33} , streamwise. (Continued)

4.2 Turbulence intensities

Turbulence intensities are shown in figures 5(a)–(c). As is well known, in pure shear channel flow, only the streamwise mean velocity exists. The streamwise velocity fluctuation is mainly generated by the shear process of the mean flow, while the mechanism to generate the spanwise velocity fluctuation is the splattering effect induced by the high-speed streaky structures rushing to the wall and the low-speed ones lifting away from the wall. Both the high- and low-speed streaky structures are related to the shear process of the mean flow [25]. However, in

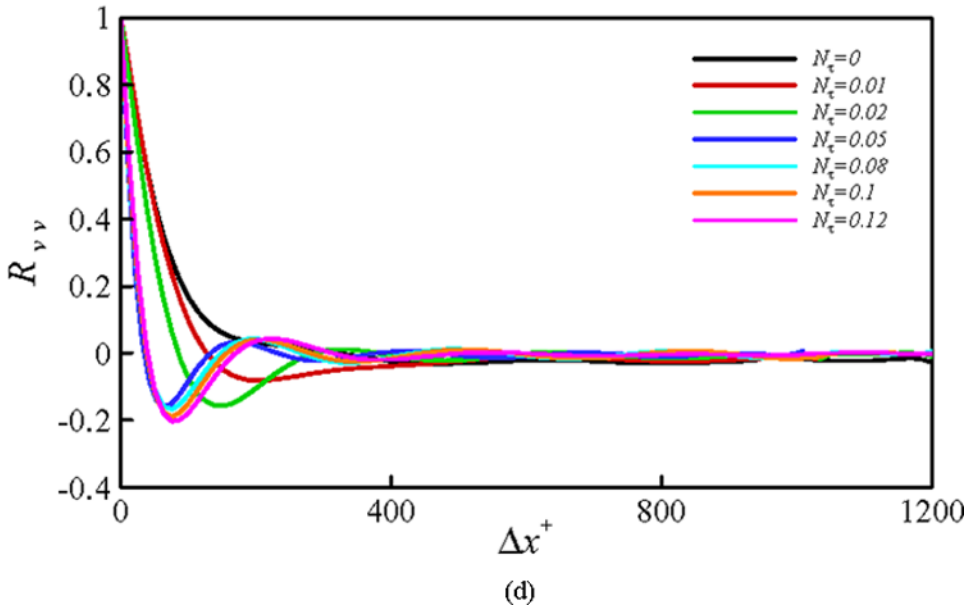
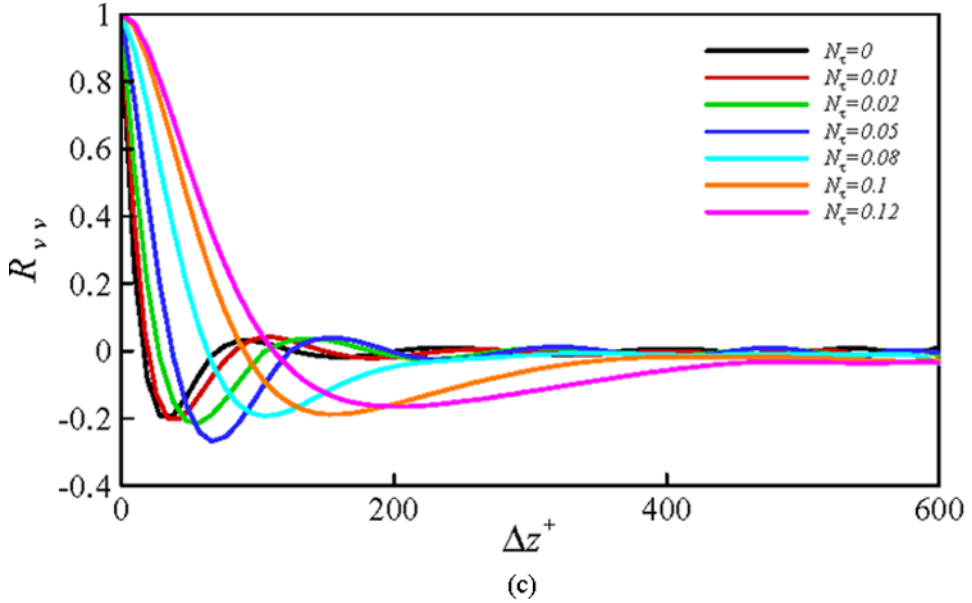


Figure 3. (Continued)

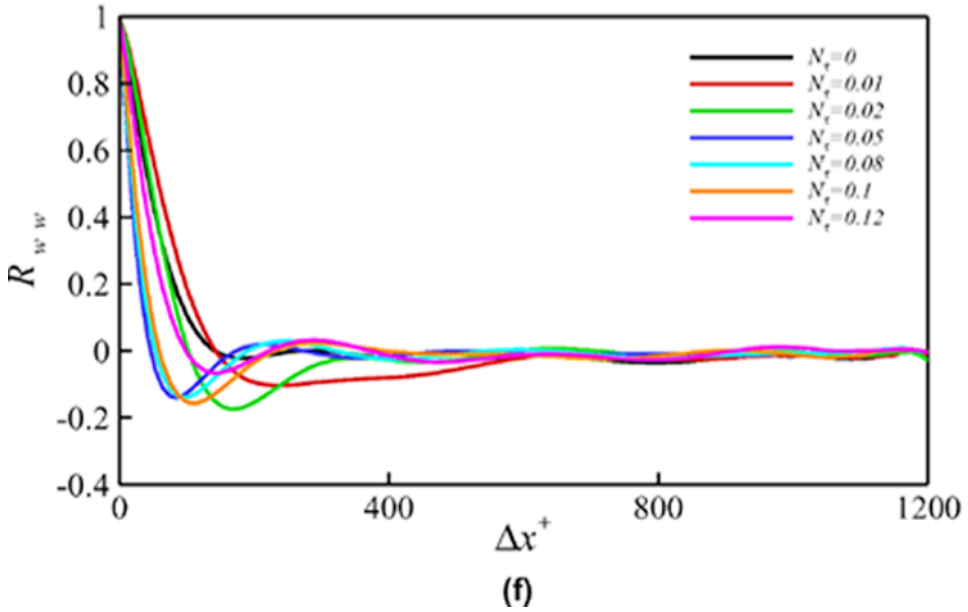
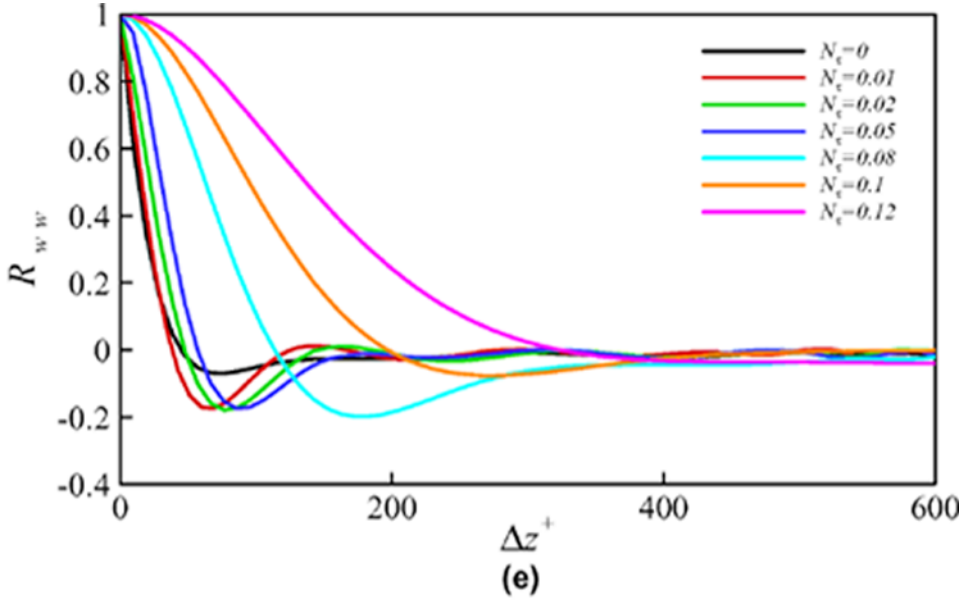


Figure 3. (Continued)

the wall-normal rotating channel, since the Coriolis force induces the spanwise mean velocity shown in figure 4(b), there exist both the streamwise and spanwise mean shear effects. Thus, the production of the streamwise turbulence fluctuation u' comes from two processes. One is the shear process related to $\langle u \rangle$, which is the major source to generate u' in the weak rotation case, and the other the splattering effect associated with $\langle w \rangle$. So does the spanwise velocity fluctuation w' , and the shear process of the spanwise mean flow will take a dominant responsibility to generate w' in the strong rotation case due to the presence of non-zero spanwise mean velocity.

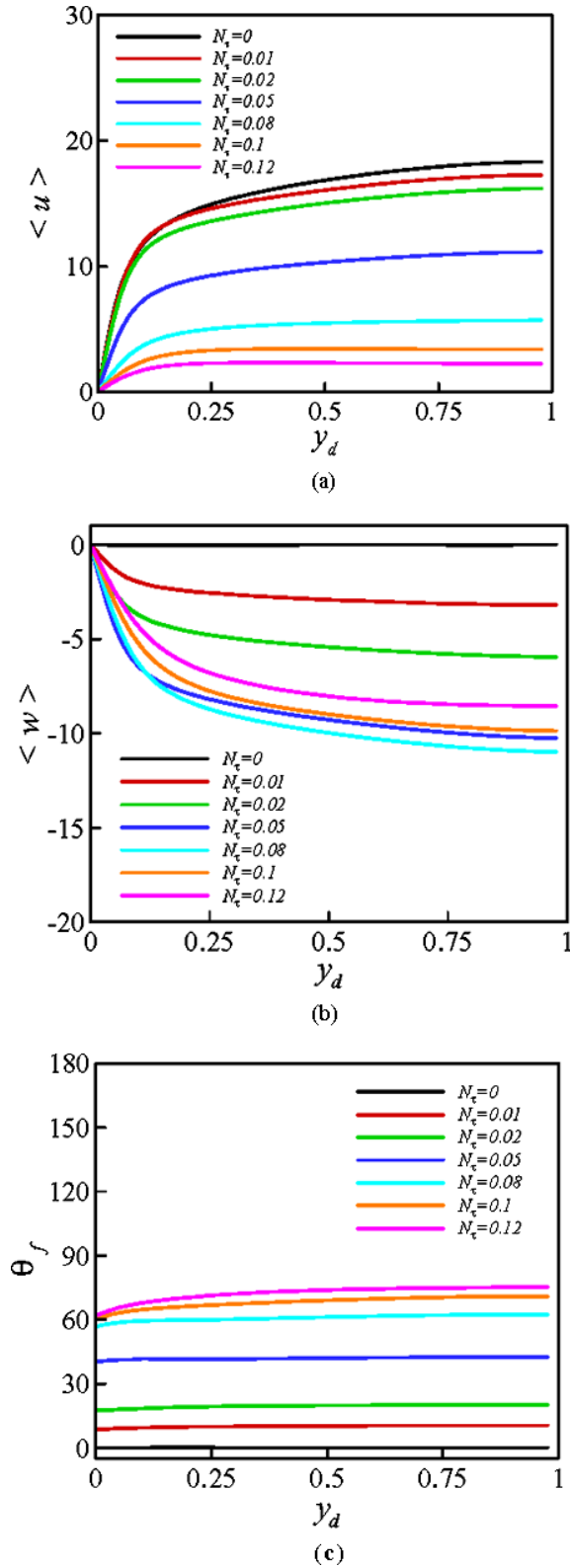
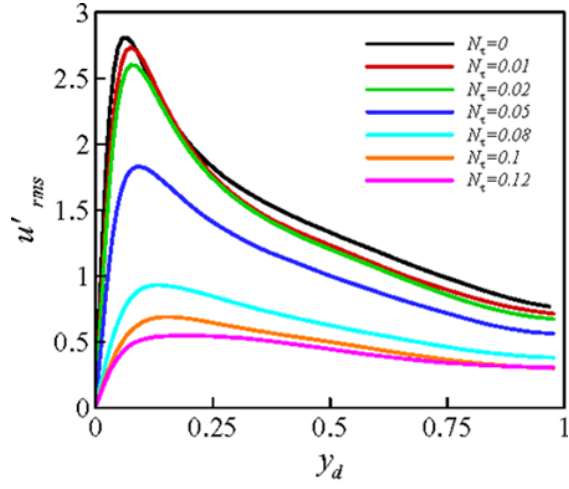
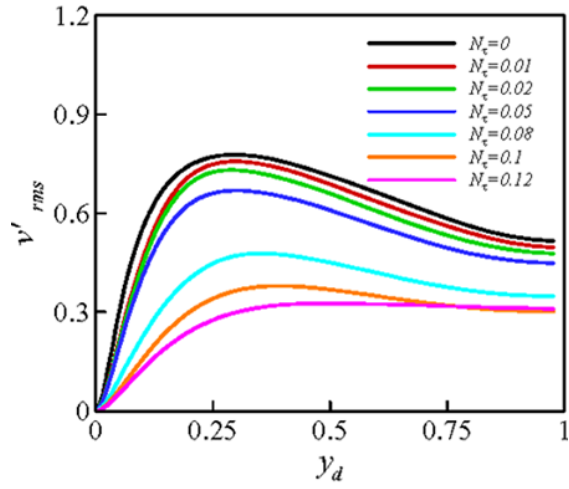


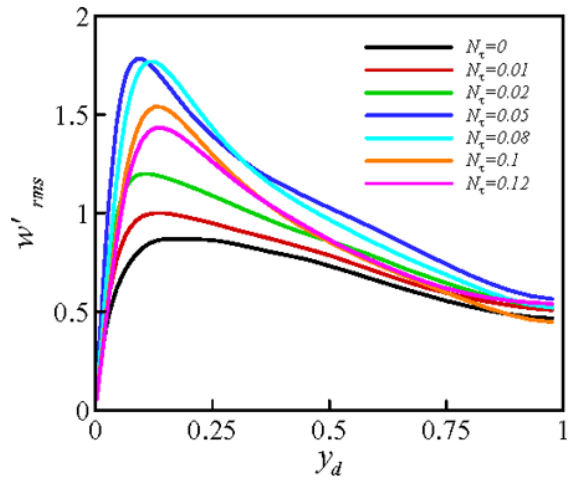
Figure 4. Profiles of the mean velocities: (a) streamwise component; (b) spanwise component; (c) angle of the absolute mean flow with respect to the streamwise direction.



(a)



(b)



(c)

Figure 5. Profiles of turbulent intensities: (a) streamwise; (b) wall-normal; (c) spanwise component.

Figure 5 shows the turbulent intensities for different rotation numbers. At low rotation number, e.g. $N_\tau = 0.01$ and 0.02 , figure 5(a) exhibits a slight reduction of u'_{rms} in the wall region, compared to that of the non-rotating case. The wall-normal turbulence intensity v'_{rms} in figure 5(b) presents a similar trend to u'_{rms} . This behaviour at low rotation number is well consistent with the findings [6, 8]. As N_τ increases further, the near-wall shear rate related to $\langle u \rangle$ reduces significantly. Thus, a rapid drop of u'_{rms} is observed in figure 5(a). When N_τ varies from 0 to 0.05, the spanwise velocity fluctuation w'_{rms} in figure 5(c) is enhanced remarkably due to increasing spanwise mean shear rate, as shown in figure 4(b). The high near-wall peak value of w'_{rms} at $N_\tau = 0.05$, compared to other rotating cases, is attributed to the strong shear rate of the spanwise mean flow, as mentioned above. When the rotation rate becomes strong, the turbulence fluctuation generation is suppressed apparently by the Coriolis force effect, which causes the reduction of all three turbulence intensities, as shown in figure 5.

4.3 Reynolds stresses

The effect of the wall-normal rotation on the turbulent channel flow is obvious to change the absolute mean flow direction, i.e. tilting to the spanwise direction shown in figure 4(c). Thus, in the wall region, the elongated streaky structures generated by the shear process of the absolute mean flow are expected to deviate from the streamwise direction and to form an acute angle with respect to the negative z -direction. This suggests that, near the bottom wall ($y/h = -1$), the high-speed (relative to the absolute mean flow) streaks, corresponding to the sweep events [18, 26], are related to the fluid with velocity fluctuations $u' > 0$, $w' < 0$ and $v' < 0$ in the rotating cases, while the low-speed streaks responsible for the ejection events correspond to $u' < 0$, $w' > 0$ and $v' > 0$. Similar conclusion can be achieved for the elongated streaks near the upper wall ($y/h = 1$). These relations between the velocity fluctuations are helpful to determine the sign of the shear stress components in the wall regions.

In figure 6, the shear stress components $\langle u'v' \rangle$ and $\langle u'w' \rangle$ are found to be negative in the bottom wall region, while $\langle v'w' \rangle$ is found to be positive, in consistent with the above description. $\langle u'v' \rangle$ is mainly connected with the change of $\langle u \rangle$ and subsequently decreases with the increase of N_τ . The weak wall-normal rotation (e.g. $N_\tau = 0.01$ and 0.02) results in slight alteration of $\langle u'v' \rangle$. As N_τ increases further to 0.1 and 0.12, $\langle u'v' \rangle$ becomes nearly zero over the channel, indicating a poor correlation between the streamwise and wall-normal velocity fluctuations subjected to a strong rotation. The distributions of $\langle u'v' \rangle$ and $\langle v'w' \rangle$ also exhibit a linear region in the core region of the channel in the rotating cases. This behaviour of $\langle u'v' \rangle$ and $\langle v'w' \rangle$ should be ascribed to the co-existence of the streamwise and spanwise mean flows in the rotating cases. $\langle v'w' \rangle$, which is connected with the change of $\langle w \rangle$, is enhanced as N_τ varies from 0 to 0.05 and suppressed as N_τ varies from 0.05 to 0.12. As shown in figure 6(c) for the profiles of $\langle u'w' \rangle$, similar trend versus N_τ is observed. These near-wall alterations of $\langle v'w' \rangle$ and $\langle u'w' \rangle$ are attributed to the shear rate of the spanwise mean flow, which contributes directly to the production rate of both the shear stress components, as predicted by the transport equation of the Reynolds stress tensor. The profiles of $\langle v'w' \rangle$ and $\langle u'w' \rangle$ show clearly a dependence on the spanwise mean flow shear rate in figures 6(b) and (c); they are strengthened for N_τ from 0 to 0.05 and weakened for N_τ from 0.05 to 0.12.

4.4 Vorticity fluctuations

The spanwise mean flow induced by the Coriolis force in the wall-normal rotating channel gives rise to the non-zero streamwise mean vorticity $\langle \omega_1 \rangle$. Thus, it must also contribute to

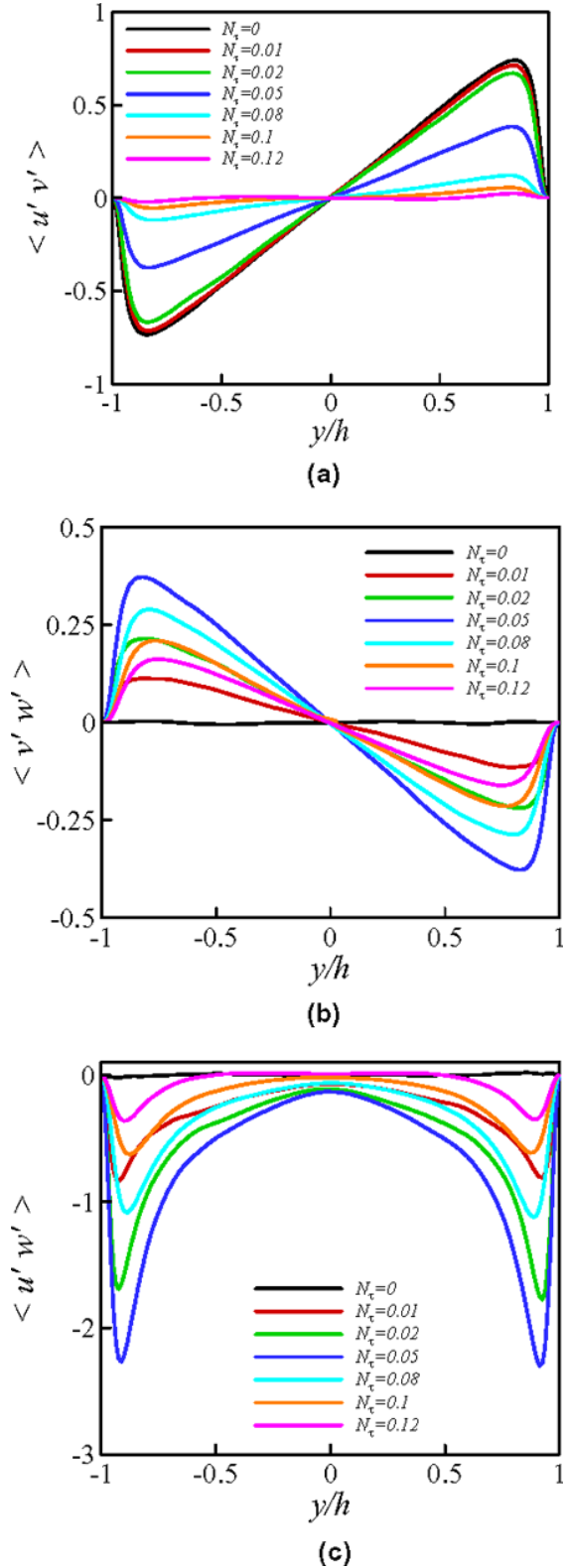
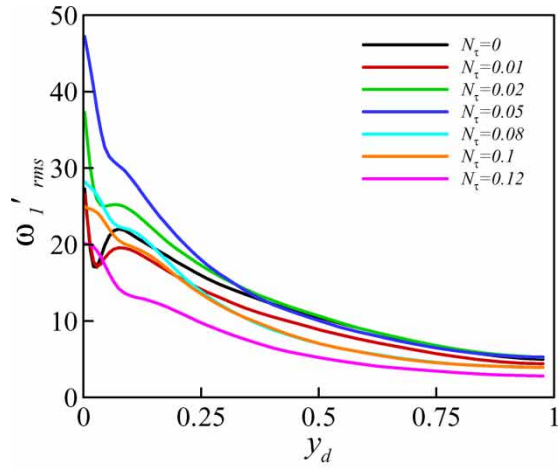
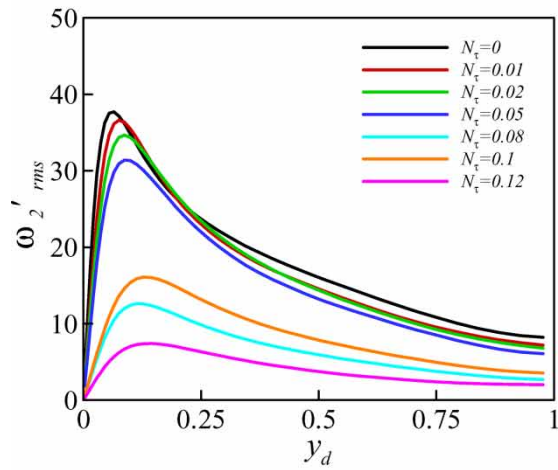


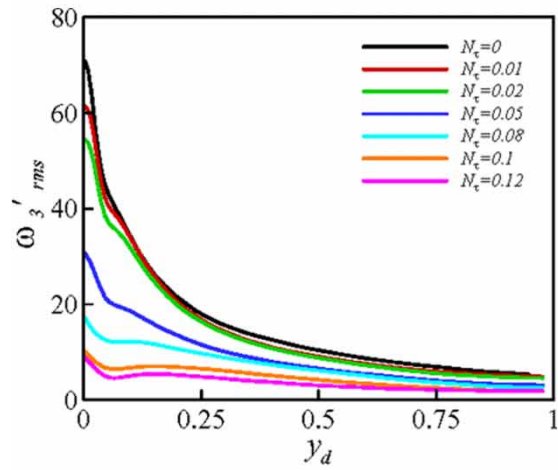
Figure 6. Distributions of the shear stress components: (a) $\langle u'v' \rangle$; (b) $\langle v'w' \rangle$; (c) $\langle u'w' \rangle$.



(a)



(b)



(c)

Figure 7. Profiles of the root-mean-square (rms) value of vorticity: (a) streamwise; (b) wall-normal; (c) spanwise component.

changing the near-wall vorticity fluctuations. The root-mean-square (rms) values of the vorticity fluctuations are depicted in figures 7(a)–(c). The definition of the streamwise vorticity fluctuation, i.e. $\omega'_1 = \partial w'/\partial y - \partial v'/\partial z$, indicates that ω'_1 is mainly dominated by the wall-normal gradient of the spanwise velocity fluctuation w' . As exhibited in figure 7(a), $\omega'_{1\text{rms}}$ is enhanced greatly for N_τ from 0 to 0.05 and suppressed for N_τ from 0.05 to 0.12.

According to the assumption of the Rankine vortex model proposed by Kim *et al.* [18], the disappearance of the local maximum and minimum of $\omega'_{1\text{rms}}$ is ascribed to the modification of the size of quasi-streamwise vortical structures in the wall region of the rotating channel. Considering the definition of the wall-normal component of the vorticity fluctuation, $\omega'_2 = \partial u'/\partial z - \partial w'/\partial x$, the trend of $\omega'_{2\text{rms}}$ should be attributed to the intensity of high- and low-speed streaky structures, linked to u' and w' , and to the separation along the streamwise and spanwise directions between the near-wall streaks. In the weak rotation cases (i.e. $N_\tau = 0.01$ and 0.02), $\omega'_{2\text{rms}}$ decreases slightly in the wall region due to a weak reduction of u'_{rms} and a significant increase of the streamwise separation of the near-wall streaks, which will be discussed in the following. When N_τ increases further, the profiles of $\omega'_{2\text{rms}}$ drop remarkably, in particular at $N_\tau = 0.1$ and 0.12, consistent with the totally suppressed u'_{rms} and w'_{rms} .

Correspondingly, $\omega'_{3\text{rms}}$ is related to the variation of u'_{rms} based on the definition of $\omega'_{3\text{rms}}$. Thus, as shown in figure 7(c), $\omega'_{3\text{rms}}$ demonstrates a reasonable trend versus N_τ ; it decreases subsequently as the rotation rate becomes stronger. In the strong rotation case (e.g. $N_\tau = 0.1$ and 0.12), local minimum and maximum of $\omega'_{3\text{rms}}$ are observed in the wall region, similar to the distribution of $\omega'_{1\text{rms}}$ in the non-rotating case. This fact implies the presence of quasi-spanwise vortical structures near the wall, since the spanwise mean flow induced by the strong rotation prevails over the streamwise one.

4.5 Turbulence budgets

The Reynolds stress budgets are helpful in understanding the rotation effect on dynamical characteristics of turbulence based on the production rate, redistribution and dissipation rate of turbulent kinetic energy. Here, our aim is to examine the influence of the wall-normal rotation on the turbulence budgets, in particular in the wall region.

The non-dimensional budgets of Reynolds stresses for the incompressible flow are given as

$$\frac{\partial \langle u'_i u'_j \rangle}{\partial t} + \langle u_k \rangle \frac{\partial \langle u'_i u'_j \rangle}{\partial x_k} = P_{ij} + T_{ij} + D_{ij} + \Pi_{ij} + \pi_{ij} + \varepsilon_{ij} + N_{ij}. \quad (7)$$

The terms on the right-hand side of equation (7) are described as follows:

$$\begin{aligned} P_{ij} &= - \left[\langle u'_i u'_k \rangle \frac{\partial \langle u_j \rangle}{\partial x_k} + \langle u'_j u'_k \rangle \frac{\partial \langle u_i \rangle}{\partial x_k} \right] && \text{production rate (PR)} \\ T_{ij} &= - \frac{\partial \langle u'_i u'_j u'_k \rangle}{\partial x_k} && \text{turbulent diffusion (TD)} \\ D_{ij} &= - \frac{1}{\text{Re}_\tau} \frac{\partial^2 \langle u'_i u'_j \rangle}{\partial x_k \partial x_k} && \text{viscous diffusion (VD)} \\ \Pi_{ij} &= - \left[\frac{\partial \langle p' u'_i \rangle}{\partial x_j} + \frac{\partial \langle p' u'_j \rangle}{\partial x_i} \right] && \text{pressure-velocity diffusion (PV)} \\ \pi_{ij} &= \left\langle p' \left(\frac{\partial u'_i}{\partial x_j} + \frac{\partial u'_j}{\partial x_i} \right) \right\rangle && \text{pressure strain correlation (PS)} \end{aligned}$$

$$\varepsilon_{ij} = -\frac{2}{\text{Re}_\tau} \left\langle \frac{\partial u'_i}{\partial x_k} \frac{\partial u'_j}{\partial x_k} \right\rangle \quad \text{dissipation rate (DS)}$$

$$N_{ij} = -N_\tau \Omega_l (\varepsilon_{ilk} \langle u'_k u'_j \rangle + \varepsilon_{jlk} \langle u'_k u'_i \rangle) / \Omega \quad \text{Coriolis force velocity correlation (CO)}$$

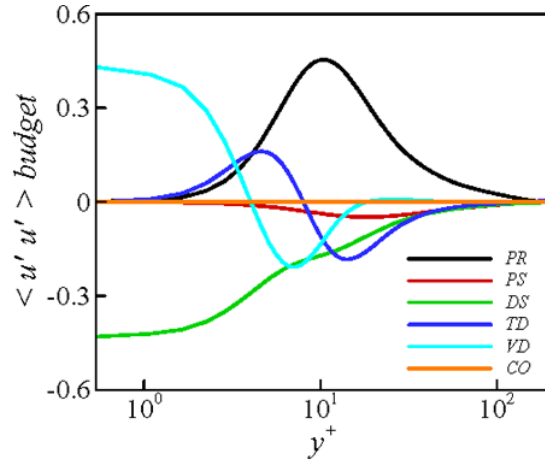
where repeated indices represent the summation over 1, 2, 3, corresponding to the streamwise, wall-normal and spanwise directions, respectively. Here, we mainly concern the budgets of $\langle u'u' \rangle$ and $\langle w'w' \rangle$ to investigate the effect of the wall-normal rotation on the dynamic processes of turbulence energy. The term Π_{ij} in the budgets of $\langle u'u' \rangle$ and $\langle w'w' \rangle$ vanishes, since we have assumed that the flow is homogeneous in the streamwise and spanwise directions. The budget terms for $N_\tau = 0, 0.05$ and 0.12 are exhibited. All the budget terms are re-scaled by u_τ^4/ν , as suggested by Mansour *et al.* [27].

The budget terms of $\langle u'u' \rangle$ at $N_\tau = 0, 0.05$ and 0.12 are shown in figures 8(a)–(c), respectively. An overview in figure 8 is the remarkable reduction of all the budget terms in the rotating cases, indicating the decrease of the streamwise turbulence fluctuation. The positive production rate P_{11} , as shown in figures 9(a) and (b), plays a major role for the generation of the streamwise velocity fluctuation by the shear process of the streamwise mean flow [26] and contributes greatly to the $\langle u'u' \rangle$ budget in the region $y^+ \approx 10$ at $N_\tau = 0$ and 0.05 . The pressure strain correlation π_{11} , responding to the energy redistribution [28], is negative in figure 8(a); it represents that π_{11} drains energy from the streamwise velocity fluctuation to the other two components in the non-rotating case. However, at $N_\tau = 0.12$ in figure 9(c), it is noted that the production rate P_{11} is overridden by the positive π_{11} . This feature indicates that increasing the wall-normal rotation alters the mechanism of the generation of the streamwise turbulent energy, which is shear production due to the streamwise mean flow in the non-rotating case. However, the energy redistribution is closely related to the pressure strain correlation in the strong rotation case.

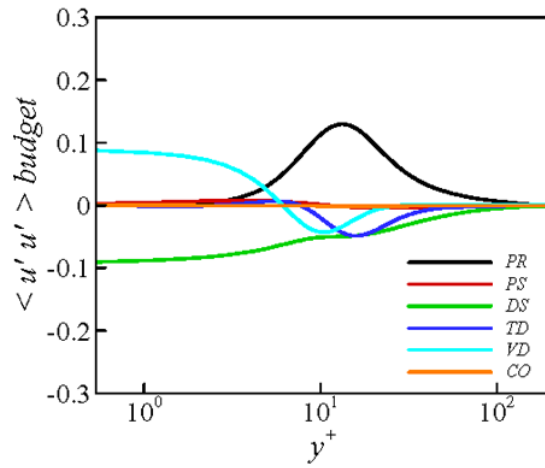
The levelling off of P_{11} in the rotating cases, as shown in figure 9(a), is formed by the decrease of the streamwise mean shear rate $\partial \langle u \rangle / \partial y$ and the Reynolds stress $\langle u'v' \rangle$, as mentioned above. In the near wall region, the balance of the $\langle u'u' \rangle$ budget is mainly due to the interaction between D_{11} and ε_{11} . Both the terms behave in a similar manner to P_{11} when N_τ increases, as shown in figures 9(b) and (c). Special attention is paid to the Coriolis force velocity correlation term, since it accounts for the energy redistribution between the streamwise and spanwise turbulence fluctuations. The negative value of N_{11} in figure 9(d) suggests that this term drains turbulent kinetic energy from the streamwise to spanwise fluctuation, even though it contributes somewhat small in the $\langle u'u' \rangle$ budget, as shown in figures 8(a)–(c).

Obvious difference is exhibited in figures 10(a)–(c), by comparing the budget terms of $\langle w'w' \rangle$ in the non-rotating case to those at $N_\tau = 0.05$ and 0.12 . In pure shear channel flow (i.e. $N_\tau = 0$), since the production rate P_{33} is absent, the positive π_{33} acts as a source term to generate the spanwise velocity fluctuation over the channel by the energy redistribution process [25, 27]. In the region very close to the wall, D_{33} and ε_{33} are responsible for the balance of the $\langle w'w' \rangle$ budget. However, as the channel rotates, due to the presence of the spanwise mean flow, the $\langle w'w' \rangle$ budget terms behave as those in $\langle u'u' \rangle$ in figure 8(a), in particular at $N_\tau = 0.12$. By comparing figures 10(a)–(c), the mechanism for the generation of the spanwise velocity fluctuation is found to be the shear production associated with P_{33} for the strong rotation case other than the energy redistribution due to π_{33} for the non-rotating case. In figure 10(c), the negative π_{33} at $N_\tau = 0.12$ implies the dynamic process to drain kinetic energy from the spanwise turbulence fluctuation.

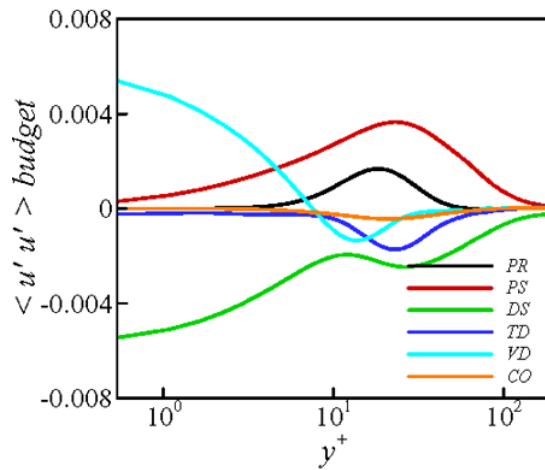
Figures 11(a)–(c) show the dependence of P_{33} , D_{33} and ε_{33} on the spanwise mean shear rate. They are strengthened for N_τ from 0 to 0.05 and suppressed for N_τ from 0.05 to 0.12.



(a)



(b)



(c)

Figure 8. Distributions of the budget terms in the transport equation of $\langle u'u' \rangle$: (a) $N_\tau = 0$; (b) $N_\tau = 0.05$; (c) $N_\tau = 0.12$.

These three terms are the vital contributions to the $\langle w'w' \rangle$ budgets in the strong rotation case. The pressure strain correlation (π_{33}) presents a different trend from those of P_{33} , D_{33} and ε_{33} observed in figure 11(d), representing a gradual reduction for N_τ from 0 to 0.05. If the wall-normal rotation is weak (i.e. $N_\tau < 0.05$), π_{33} remains nearly positive over the channel, redistributing turbulent kinetic energy to the spanwise turbulence fluctuation. However, different situation appears as N_τ increases further; π_{33} changes to be negative subjected to a strong rotation. Thus turbulent kinetic energy is redistributed to the streamwise and wall-normal turbulence fluctuation by π_{33} .

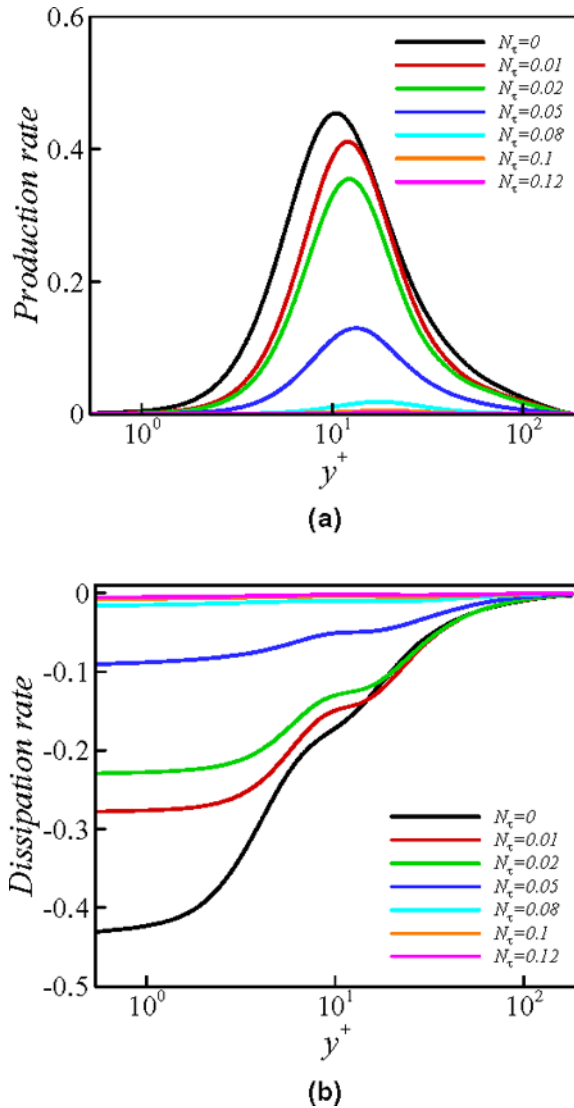
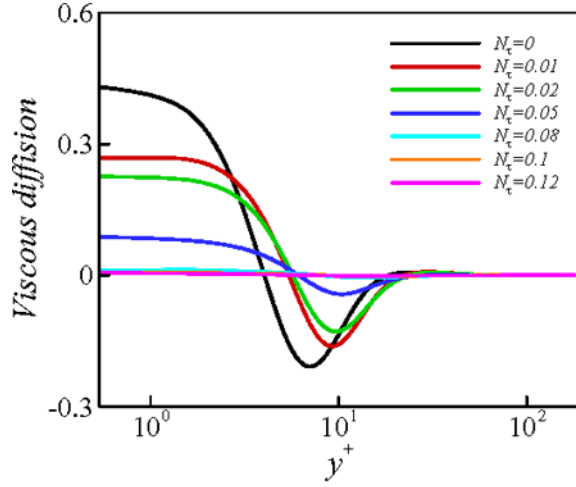
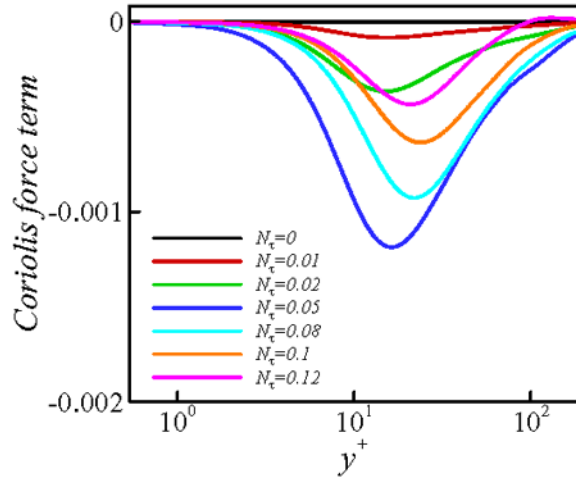


Figure 9. Budget terms in the transport equation of $\langle u'u' \rangle$: (a) production rate (PR); (b) dissipation rate (DS); (c) viscous diffusion (VD); (d) Coriolis force term (CO). (Continued)



(c)



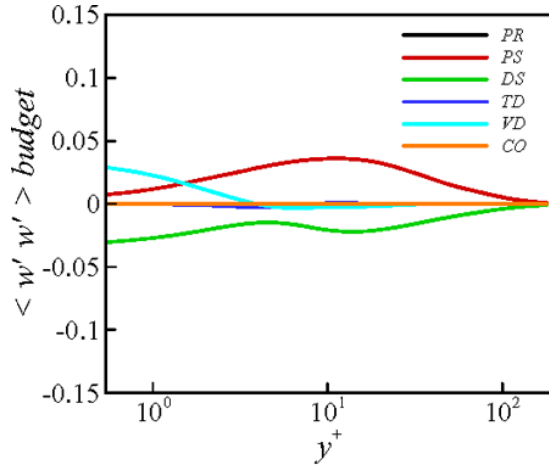
(d)

Figure 9. (Continued)

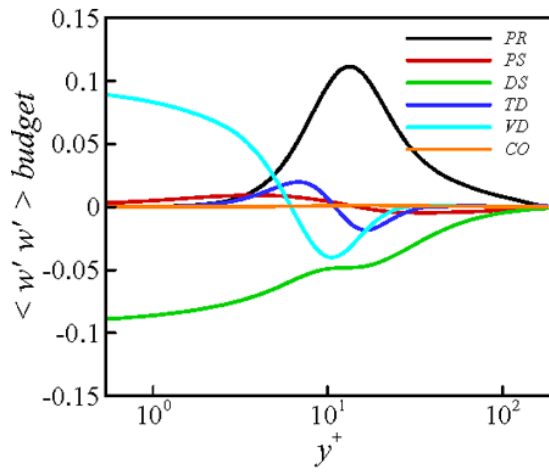
4.6 Flow structures

As shown in figures 12(a) and (b) for the contours of the streamwise velocity fluctuation u' , the reduction of u' at $N_\tau = 0.05$ is observed, since dense elongated streaky structures in the contour plots of u' appear in the non-rotating channel wall region. The inclined direction of the near-wall structures is clearly exhibited. The corresponding structures based on the wall-normal fluctuation v' and the spanwise fluctuation w' are also examined. The behaviour exhibited in the flow structures is well consistent with the turbulence intensities shown in figures 4(a)–(c).

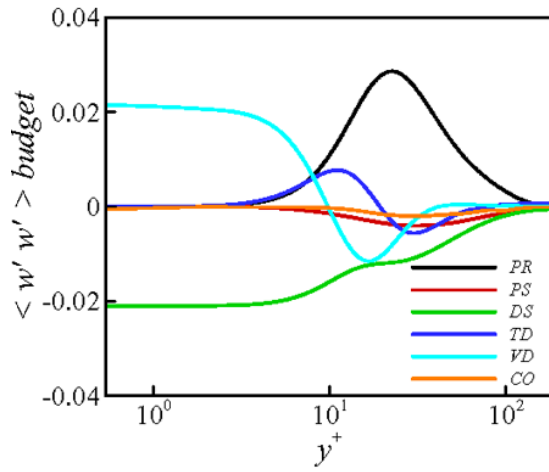
The contours of the velocity fluctuations also demonstrate the alteration of the streamwise and spanwise separations between the wall streaky structures, compared to the non-rotating case. In pure shear channel flow, the streaky structures are exactly aligned with the streamwise



(a)



(b)



(c)

Figure 10. Distributions of the budget terms in the transport equation of $\langle w'w' \rangle$: (a) $N_\tau = 0$; (b) $N_\tau = 0.05$; (c) $N_\tau = 0.12$.

direction, arranged in the spanwise direction. This fact accounts for the distributions of the two-point correlations of the velocity fluctuations, i.e. R_{uu} , R_{vv} and R_{ww} , gradually falling off to zero along the streamwise direction but exhibiting a distinct minimum along the spanwise direction, as shown in figures 3(a)–(f). In the rotating cases, the streaky structures are nearly aligned with the absolute mean flow, which results in finite streamwise separation between the wall streaks, as shown in figure 12. Consequently, distinct minima occur not only in the distributions of R_{uu} , R_{vv} and R_{ww} along the spanwise direction but also in those along the streamwise direction, as shown in figures 3(a)–(f). In figures 3(a)–(f), the spanwise separations at which the minima of R_{uu} , R_{vv} and R_{ww} occur increase monotonically with the increase of N_τ , indicating the subsequent increase of the spanwise spacing between the streak structures. It is interesting to note that the streamwise separations corresponding to the

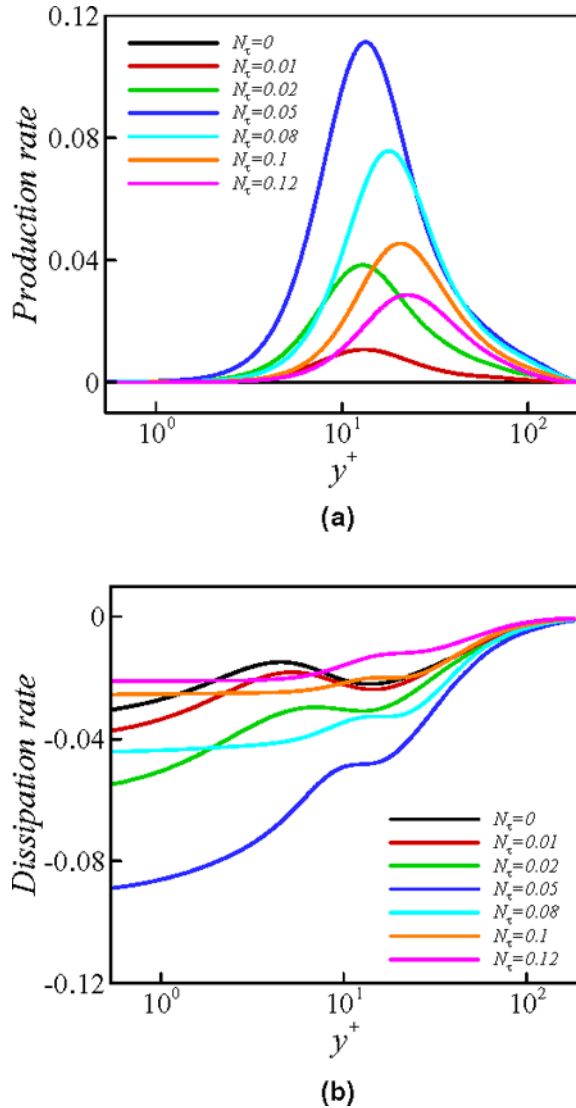
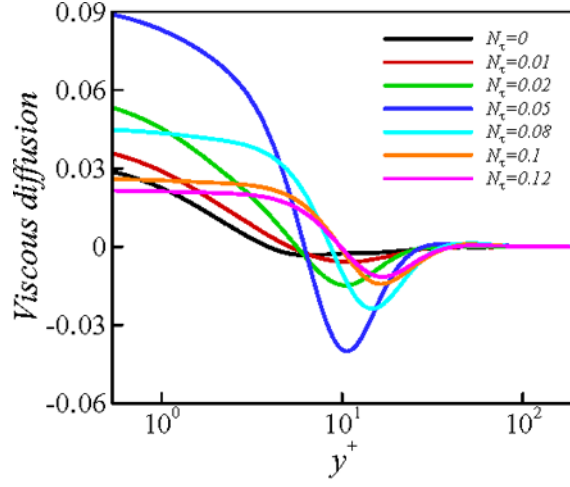
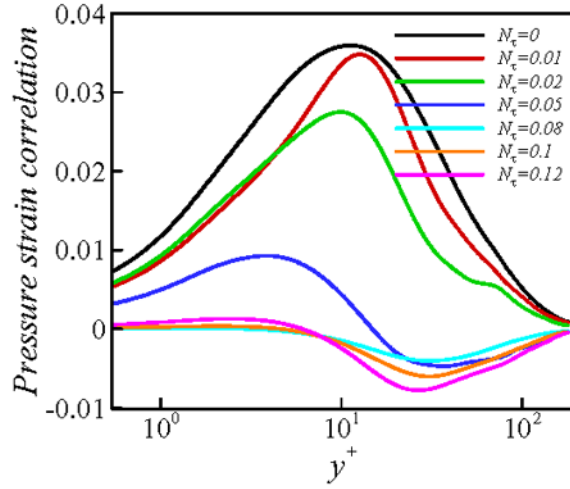


Figure 11. Budget terms in the transport equation of $\langle w'w' \rangle$: (a) production rate (PR); (b) dissipation rate (DS); (c) pressure strain correlation (PS); (d) viscous diffusion (VD). (Continued)



(c)



(d)

Figure 11. (Continued)

minima of R_{uu} , R_{vv} and R_{ww} also show a dependence on the spanwise mean shear rate; they decrease when N_τ varies from 0 to 0.05 and increase when N_τ increases further, as shown in figures 3(a)–(f).

According to Kim *et al.* [18], the mean spacing between the streaky structures is defined as twice the spanwise separation corresponding to the minimum R_{uu} in the non-rotating channel flow. The definition also provides an estimate of the mean spacing between the streaky structures in the wall-normal rotating cases. As illustrated in figure 13, if the spanwise and streamwise separations corresponding to the minima of R_{uu} along the spanwise and streamwise directions are denoted as λ_z^+ and λ_x^+ , respectively, then the mean spacing λ^+ can be obtained by

$$\lambda^+ = 2\lambda_z^+\lambda_x^+/\sqrt{\lambda_z^{+2} + \lambda_x^{+2}}. \quad (8)$$

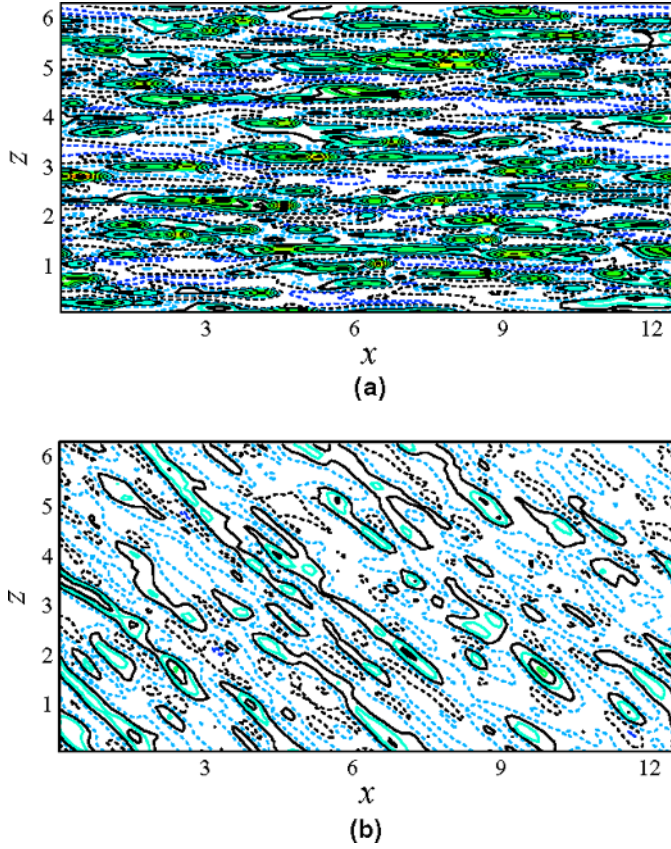


Figure 12. Contours of the instantaneous streamwise velocity fluctuation in the (x, z) plane at $y^+ = 5.4$: (a) $N_\tau = 0$; (b) $N_\tau = 0.05$. Here, the increment of contours is 0.05.

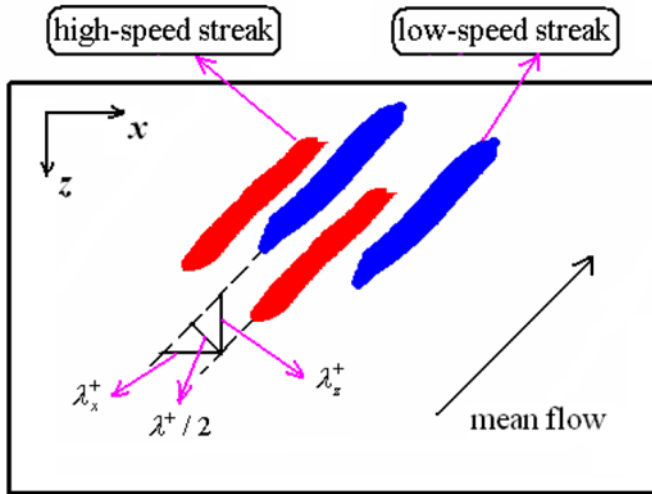


Figure 13. Sketch of the near-wall streaky structures in the wall-normal rotating channel.

Table 1. Mean spacing between the wall structures and the inclined angles of the streaky structures and the absolute mean flow.

N_τ	0	0.01	0.02	0.05	0.08	0.1	0.12
λ_z^+	53.33	61.01	67.01	85.26	148.83	205.80	275.29
λ_x^+	—	428.31	215.06	103.87	111.28	120.89	138.18
λ^+	106.66	120.80	127.95	131.80	178.24	208.47	246.99
θ_λ	0°	8.10°	17.31°	39.38°	53.21°	59.57°	63.35°
θ_f	0°	8.95°	17.61°	40.87°	55.03°	60.32°	64.27°

It is found that the mean spacing between the streaky structures near the wall exhibits slight augment in the weak rotation case, but increases considerably as the rotation rate becomes stronger, as listed in table 1. The mean angle between the streaky structures and the streamwise direction can be evaluated by

$$\theta_\lambda = \tan^{-1}(\lambda_z^+/\lambda_x^+). \quad (9)$$

Table 1 also lists the corresponding angle θ_λ . Compared to the angle obtained by the mean flow (θ_f) at the same (x, z) plane, it is identified that the streaky structures are basically in alignment with the absolute mean flow although some discrepancy between θ_λ and θ_f appears.

5. Concluding remarks

Fully developed turbulent flow in a wall-normal rotating channel is investigated by means of DNS. When the channel flow is subjected to the wall-normal rotation, the influence of the Coriolis force is examined for the rotation number ranging from weak (e.g. $N_\tau = 0.01$) to strong rotation (e.g. $N_\tau = 0.12$). Turbulence statistical quantities are found to suffer two rotation regimes as N_τ increases from 0 to 0.12. When N_τ increases from 0 to 0.05, the turbulence statistics correlated with the spanwise velocity fluctuation are strengthened due to increasing shear rate of the spanwise mean flow, but other statistics decrease subsequently. While $N_\tau > 0.05$, all the turbulence statistics diminish significantly due to the Coriolis force effect. The dependence on the spanwise mean shear rate, increasing for N_τ from 0 to 0.05 and then decreasing for N_τ from 0.05 to 0.12, is observed in statistical quantities correlated with the spanwise velocity fluctuation. The budgets of $\langle u'u' \rangle$ and $\langle w'w' \rangle$ exhibit the alteration of the dominant mechanisms to generate the streamwise and spanwise turbulence fluctuations with the increase of N_τ . For the streamwise velocity fluctuation, the dominant mechanism changes from shear production linked to the streamwise mean flow to the energy redistribution due to the pressure strain correlation; for the spanwise one, however, it alters from the energy redistribution to the shear production due to the rotation-induced spanwise mean flow. The energy redistribution due to the Coriolis force contributes somewhat little to the generation of the turbulent fluctuations. The near-wall streaky structures, redirected by the Coriolis force effect, are proved to be in alignment with the absolute mean flow in the rotating cases. The redirection of the turbulence structures is responsible for the distributions of two-point correlations of the velocity fluctuations and results in the increase of the mean spacing (λ^+) between the high- and low-speed elongated streaks. The evaluation of λ^+ reflects an appreciable increase of the separation between the streaky structures when the wall-normal rotation rate increases.

Acknowledgements

This work was supported by the National Natural Science Foundation of China (Nos. 10302028, 90405007, 10125210), the Hundred Talents Program of the Chinese Academy of Sciences (CAS), and Specialized Research Fund for the Doctoral Program of Higher Education (No. 20020358013).

References

- [1] Johnston, J.P., Halleen, R.M. and Lezius, D.K., 1972, Effects of spanwise rotation on the structure of two-dimensional fully developed turbulent channel flow. *Journal of Fluid Mechanics*, **56**, 533–557.
- [2] Nakabayashi, K. and Kitoh, O., 1996, Low Reynolds number fully developed turbulent channel flow with system rotation. *Journal of Fluid Mechanics*, **315**, 1–29.
- [3] Piomelli, U. and Liu, J., 1995, Large-eddy simulation of rotating channel flows using a localized dynamic model. *Physics of Fluids*, **7**, 839–848.
- [4] Kristoffersen, R. and Andersson, H.I., 1993, Direct simulations of low-Reynolds number turbulent flow in a rotating channel. *Journal of Fluid Mechanics*, **235**, 163–197.
- [5] Nagano, Y. and Hattori, H., 2002, An improved turbulence model for rotating shear flow. *Journal of Turbulence*, **3**, 6.
- [6] Elsamni, O. and Kasagi, N., 2001, The effects of system rotation with three orthogonal rotating axes on turbulent channel flow. *Proc. 7th Int. Congress Fluid Dynamics Propulsion*, Cairo, Egypt, 18–20 December 2001, CD-ROM.
- [7] Esau, I., 2003, The Coriolis effect on coherent structures in planetary boundary layers. *Journal of Turbulence*, **4**, 17.
- [8] Wu, H.B. and Kasagi, N., 2004, Effects of arbitrary directional system rotation on turbulent channel flow. *Physics of Fluids*, **16**, 979–990.
- [9] Lu, X.Y., Wang, S.W., Sung, H.G., Hsieh, S.Y. and Yang, V., 2005, Large eddy simulations of turbulent swirling flows injected into a dump chamber. *Journal of Fluid Mechanics*, **527**, 171–195.
- [10] Liu, N.S. and Lu, X.Y., 2005, Large eddy simulation of turbulent flows in a rotating concentric annular channel. *International Journal of Heat Fluid Flow*, **26**, 378–392.
- [11] Haeusser, T.M. and Leibovich, S., 2003, Pattern formation in the marginally unstable Ekman layer. *Journal of Fluid Mechanics*, **479**, 125–144.
- [12] Zikanov, O., Slinn, D.N. and Dhanak, M.R., 2003, Large-eddy simulations of the wind-induced turbulent Ekman layer. *Journal of Fluid Mechanics*, **495**, 343–368.
- [13] Speziale, C.G., Younis, B.A., Rubinstein, R. and Zhou, Y., 1998, On consistency condition for rotating turbulent flows. *Physics of Fluids*, **22**, 2108–2110.
- [14] Ekman, V.W., 1905, On the influence of the earth's rotation on ocean currents. *Ark. Mart. Aster. Fys.*, **2**, 1–53.
- [15] Orlandi, P., 2000, *Fluid Flow Phenomena* (Dordrecht: Kluwer).
- [16] Kim, J. and Moin, P., 1985, Application of a fractional-step method to incompressible Navier–Stokes equations. *Journal of Computational Physics*, **59**, 308–323.
- [17] Rai, M.M. and Moin, P., 1991, Direct simulations of turbulent flow using finite-difference schemes. *Journal of Computational Physics*, **96**, 15–53.
- [18] Kim, J., Moin, P. and Moser, R., 1987, Turbulence statistics in fully developed channel flow at low Reynolds number. *Journal of Fluid Mechanics*, **177**, 133–166.
- [19] Orlandi, P., 1997, Helicity fluctuations and turbulent energy production in rotating and non-rotating pipes. *Physics of Fluids*, **9**, 2045–2056.
- [20] Orlandi, P. and Fatica, M., 1997, Direct simulations of turbulent flow in a pipe rotating about its axis. *Journal of Fluid Mechanics*, **343**, 43–72.
- [21] Liu, N.S. and Lu, X.Y., 2004, Large eddy simulation of turbulent concentric annular channel flows. *International Journal for Numerical Methods in Fluids*, **45**, 1317–1338.
- [22] Dong, Y.H. and Lu, X.Y., 2004, Large eddy simulation of a thermally stratified turbulent channel flow with temperature oscillation on the wall. *International Journal of Heat Mass Transfer*, **47**, 2109–2122.
- [23] Wang, L. and Lu, X.Y., 2004, An investigation of turbulent oscillatory heat transfer in channel flows by large eddy simulation. *International Journal of Heat Mass Transfer*, **47**, 2161–2172.
- [24] Wang, L., Dong, Y.H. and Lu, X.Y., 2005, An investigation of turbulent open channel flow with heat transfer by large eddy simulation. *Computers Fluids*, **34**, 23–47.
- [25] Moin, P. and Kim, J., 1982, Numerical investigation of turbulent channel flow. *Journal of Fluid Mechanics*, **118**, 341–377.
- [26] Tennekes, H. and Lumley, L., 1972, *A First Course in Turbulence* (Cambridge, MA: MIT Press).
- [27] Mansour, N.N., Kim, J. and Moin, P., 1988, Reynolds-stress and dissipation-rate budgets in a turbulent channel flow. *Journal of Fluid Mechanics*, **194**, 15–44.
- [28] Calmet, I. and Magnaudet, J., 2003, Statistical structure of high-Reynolds-number turbulence close to the free surface of an open-channel flow. *Journal of Fluid Mechanics*, **474**, 355–378.